PREPRINT SUBMITTED

This manuscript is a preprint uploaded to EarthArXiv. This preprint has been submitted for publication to *Communications Earth & Environment* on the 30th of August 2021. Authors encourage downloading the latest manuscript version from EarthArXiv, and welcome comments, feedback and discussions anytime. Please, feel free to get in contact: gino@ginodegelder.nl

Title: High interstadial sea levels over the past 420ka from Huon terraces (Papua New Guinea)

Authors: Gino de Gelder[1*], Laurent Husson[1], Anne-Morwenn Pastier[2], David Fernández-Blanco[3], Tamara Pico[4], Denovan Chauveau[5], Christine Authemayou[5], Kevin Pedoja[6]

Affiliations:

1) ISTerre, Université Grenoble-Alpes, 1381 Rue de la Piscine, 38400 St. Martin d'Hères, France

2) GeoForschungsZentrum, Telegrafenberg, 14473 Potsdam, Germany

3) Barcelona Center for Subsurface Imaging, Passeig Marítim de Barceloneta 37-49, E-08003 Barcelona, Spain

4) California Institute of Technology, 1200 E California Blvd, Pasadena CA 91125, US

5) Université de Bretagne Occidentale, 3 Rue des Archives, 29238 Brest, France

6) Université de Caen, Espl. de la Paix, 14000 Caen, France

* Corresponding author: gino@ginodegelder.nl

High interstadial sea levels over the past 420ka from Huon terraces (Papua New Guinea)

Gino de Gelder[1*], Laurent Husson[1], Anne-Morwenn Pastier[2], David Fernández-Blanco[3], Tamara Pico[4], Denovan Chauveau[5], Christine Authemayou[5], Kevin Pedoja[6]

The history of sea level across the Quaternary is essential for assessing past and future climate and geodynamics. Global sea-level reconstructions are typically derived from oxygen isotope curves, but require calibration with geological constraints that are particularly scarce prior to the last glacial cycle (>130 ka). The exceptionally well-preserved coral reef terrace sequence in the Huon Peninsula (Papua New Guinea) may provide such constraints up to ~420 ka, but has never been analysed in its full extent, or with high-resolution topographic data. Here we apply novel geometric approaches to show that the terrace sequence deformation pattern can be approximated by a northward tectonic tilt, and estimate relative sea-level (RSL) for 31 Late Pleistocene periods, including several periods for which no other RSL data exists elsewhere. Supported by reef modelling, these estimates suggest that global mean sea-level curves derived from oxygen isotopes systematically underestimate interstadial sea-level elevations, by up to ~20m. We propose that this discrepancy is either an effect of incorrect oxygen isotope curve calibrations, or that some short-lived sea-level variations are simply not recorded in oxygen isotope ratios.

Linking past sea-level changes to climatic variations and ice-sheet configurations is fundamental to predicting future climate change scenarios[1] and understanding large-scale geodynamics[2]. The Quaternary represents a key geological archive, as it is the most recent period recording the full spectrum of glacial-interglacial sea-level changes[3]. Continuous records of past global mean sea-level (GMSL) are usually derived from oxygen isotope ratios ($\delta^{18}O$) in marine sediment cores, as the seawater ratio between the lighter (^{16}O) and heavier (^{18}O) isotopes relies on the amount of ice stored within continental ice sheets. Since temperatures and local hydrological/chemical conditions also affect $\delta^{18}O$ ratios, many calibration techniques have been proposed for the derivation of GMSL curves from $\delta^{18}O$-records, which has led to a broad range of GMSL estimates[4,5]. Commonly, to verify or adjust $\delta^{18}O$-derived sea-level curves, they are compared with reliable relative sea-level (RSL) geological indicators, corrected for Glacial Isostatic Adjustment (GIA). However, these data are sparse[6,7], rely on uncertain corrections for GIA or other processes of vertical displacement, and are mostly limited to *interglacial* periods[8] with relatively

high sea-level stands - like Marine Isotope Stages (MIS) 5e (~125 ka), 7e (~240 ka), 9e (~320 ka) and 11c (~410 ka) - and *interstadial* secondary sea-level peaks of the last glacial cycle, like MIS 3 (~45 ka), 5a (~80 ka) and 5c (~100 ka)[9]. RSL estimates of *lowstands* - the troughs between peaks - and interstadials older than 130 ka are largely unknown. This lack of reliable RSL data, combined with uncertainties in $\delta^{18}O$-based GMSL curves, hinder sea-level, ice-sheet and climatic reconstructions over large portions of the Quaternary.

Here we provide the first RSL estimates for such periods by re-visiting the canonical coral reef terrace sequence of the Huon Peninsula (Fig. 1; Papua New Guinea). At this location, high uplift rates (~0.5-3.5 mm/yr) have led to the preservation of an exceptionally complete sea-level record[10]. Whereas previous studies focused on the last glacial cycle terraces, which are easier to access and better preserved, we use high-resolution digital topography to reassess the whole terrace sequence, ~40 km wide and ~1000 m high, with a novel geometry-based approach. By re-evaluating the tectonic deformation we provide RSL data for the ~420-125 ka period for the first time while improving elevation and age estimates of previously documented sea-level highstands (~125-0 ka[11]). This data allows us to critically assess $\delta^{18}O$-derived GMSL-curves, providing a foundation for improved constraints on Quaternary sea-level oscillations and ice-sheets.

New interpretation of Huon coral reef terrace deformation

Located on the northern margin of the Huon-Finisterre Ranges on the South Bismarck Plate (Fig. 1), the Huon Peninsula coral reef terraces have provided the basis for fundamental studies on Quaternary sea-level oscillations[10,12–16]. To interpret RSL in tectonically active regions like the Huon Peninsula, it is crucial to constrain uplift rates and their spatiotemporal variability. To estimate uplift rates, the terrace formed during the MIS 5e peak (~125 ka) is generally used as a benchmark, since the global mean sea-level elevation of MIS 5e is relatively well constrained[6,17,18]. At Huon, pioneering studies combined field measurements and observations of the MIS 5e and other terraces to construct detailed uplift rate contours (blue dashed contours in Fig. 1[10]), whereas later studies simply used an uplift rate calculated from the nearest MIS 5e terrace[15,16,19]. These long-standing interpretations roughly translate as a NW-directed tilt, but this assumption has never been thoroughly verified with a large-scale geometrical analysis. A different tilt direction would imply a different uplift rate correction, and would thus affect sea-level estimates by several meters.

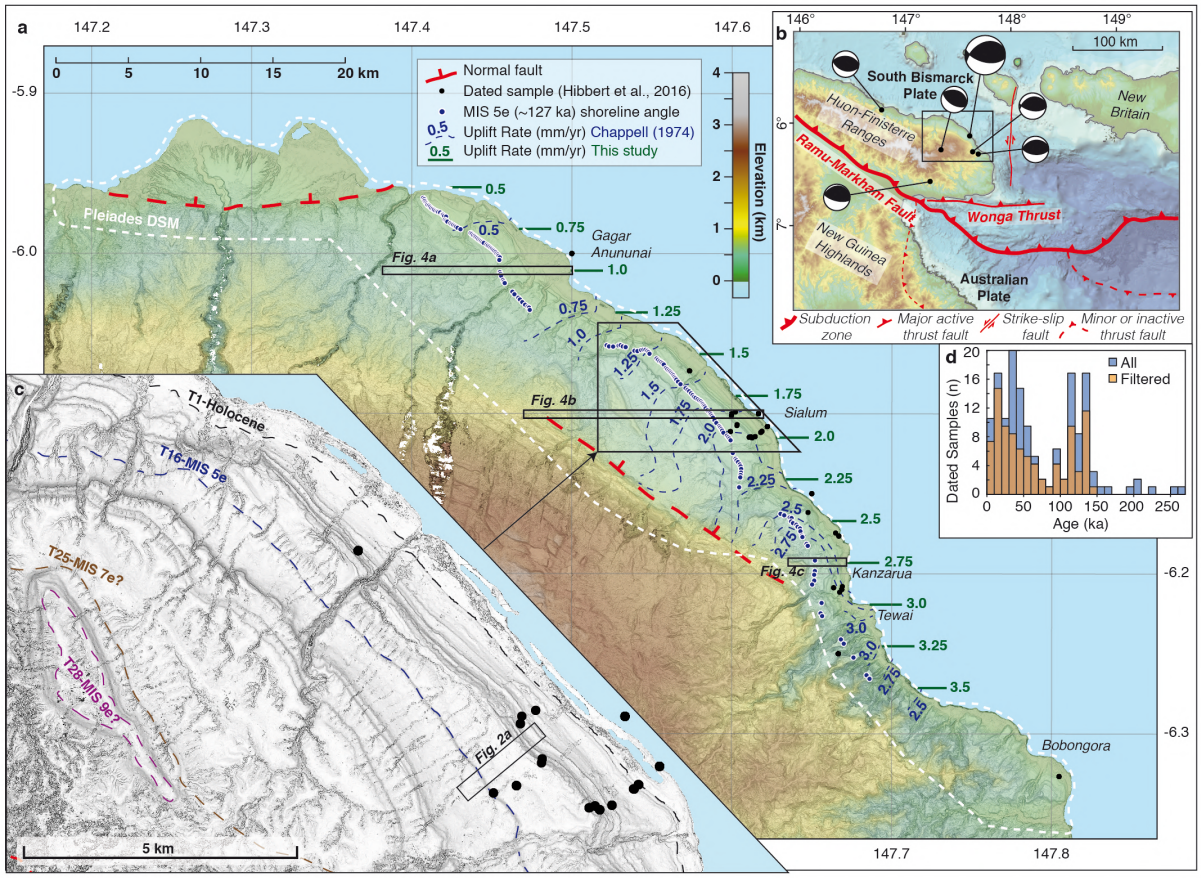

Figure 1: Uplift rates, dated samples and tectonic context of the Huon coral reef terrace sequence. a) Slope map of coral reef terrace sequence overlain with colored elevations, showing a comparison of the uplift rates proposed by Chappell et al. (1974) and this study. We also show the location of dated samples, and shoreline angles for the upper MIS 5e (~127 ka) terrace. Names in italic refer to the locations of commonly studied sections, of which 3 are modeled in Fig. 4. **b)** Regional tectonic setting, with earthquake focal mechanisms of the 1967 and 1992 seismic sequences from Abers and McCaffrey (1994) ranging from mb = 5.5 (smallest) to 6.2 (largest). **c)** Detailed DSM slope map of the Sialum area, with mapped paleoshorelines for the coral reef terraces. **d)** Ages of dated samples within the compilation of Hibbert et al. (2016). All samples in blue, and in orange the samples after removing duplicates, samples out of the study area and U/Th open system samples.

We better approximate the deformation pattern, and thus sea-level estimations, using a 2 m-resolution Digital Surface Model (DSM) derived from Pleiades satellite images (see Methods) and a 12-m resolution TanDEM-X DSM, which we use to assess the large-scale terrace geometry. As a qualitative assessment, we use hundreds of parallel topographic swaths of narrow width stacked together perpendicular to their strike[20] (hereafter termed stacked swaths[21]). Distortion of the terraces would depend on the viewing angle with respect to the dip of the terraces; minimizing the distortion of the terrace sequence indicates a N-ward directed tilt (Fig. 3a; Supplementary Fig. 1). As a quantitative assessment of this tilt, we systematically measured the elevation of the two most continuous terraces in the sequence (Supplementary Fig. 2), previously assigned to the MIS 5a and 5e highstands[19]. We specifically tracked the shoreline angle elevation, at the intersection between a terrace flat and its corresponding paleo-seacliff landwards (Fig. 2a), as a morphological approximation of paleo-RSL[22]. Using least-square functions for linear surface fitting, the ~350 measured shoreline angles (Supplementary Data 1) confirm that both terraces are almost exactly N-ward tilted (respectively N002E and N359E; Fig. 2; Supplementary Fig. 2). This tilt direction, ~45 degrees clockwise from the previously assumed NW-directed tilt, better fits the regional tectonic context, given (i) the N-S compression indicated by focal mechanisms of the region's largest earthquakes, and (ii) the E-W orientation of the Wonga Thrust immediately S of the Huon Peninsula (Fig. 1).

Inferred relative sea-levels

This improved tectonic interpretation implies different uplift-rate corrections and, more importantly, different RSL estimates with respect to previous work[11]. Specifically, compared to a NW-tilt a N-tilt should increase and decrease the elevations of pre- and post-MIS 5e RSL estimates, respectively. We calculate RSL directly from the terrace geometry, taking advantage of the linearity of the shoreline angles. If the deformation pattern and uplift rates have remained constant in time, the slopes of the terraces in across-strike W-ward view (as in Fig. 3a,b) should be proportional to the terrace ages, and extrapolation to a 0 mm/yr uplift rate should give the RSL elevation during terrace formation. We performed this calculation (see Methods) for 31 terraces (T1-T31; Fig. 3b), which we traced using the Pleiades DSM, and constitutes a major expansion from the ~20 previously recognized terraces[10,11]. Instead of using a nomenclature based on reef structure[10], on which we have no direct observations, we opted for a simpler designation of terrace numbers (T1-T31; Fig. 3; Supplementary Table 1). To calculate the regional uplift rate pattern we used an age of 127±2 ka, as previously used for the uppermost MIS 5e Huon terrace[11],

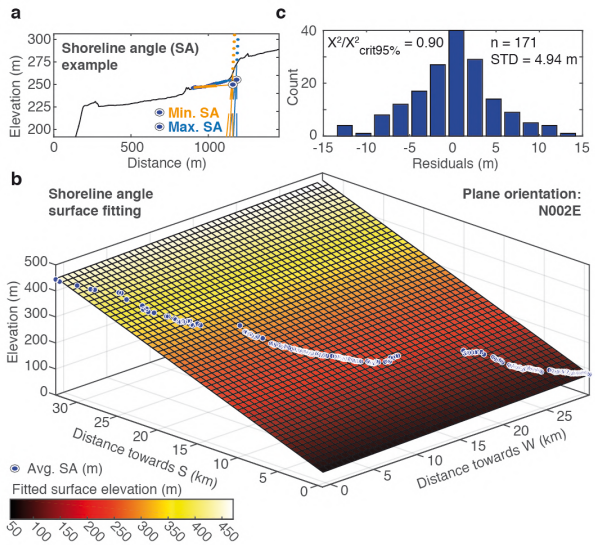

Figure 2: Best-fitting tilt direction of Huon coral reef terrace sequence. a) Example of shoreline angle determination, at the intersection between terrace and paleo-cliff, using a free-cliff analysis (De Gelder et al., 2015). Black line marks the maximum elevation of the swath profile in Fig. 1c. The orange and blue lines represent a minimum and maximum approximation, respectively, to derive the shoreline angle elevation. **b)** Linear surface fitting of MIS 5e shoreline angle elevations (blue dots), using the average values of the minima and maxima derived as in **a**. Results indicate a simple planar tilt approximately N-ward (N002E) **c)** Histogram of residuals of surface fitting including standard deviation (STD), with distribution not significantly different from Gaussian at 95% confidence as suggested by a X2 test.

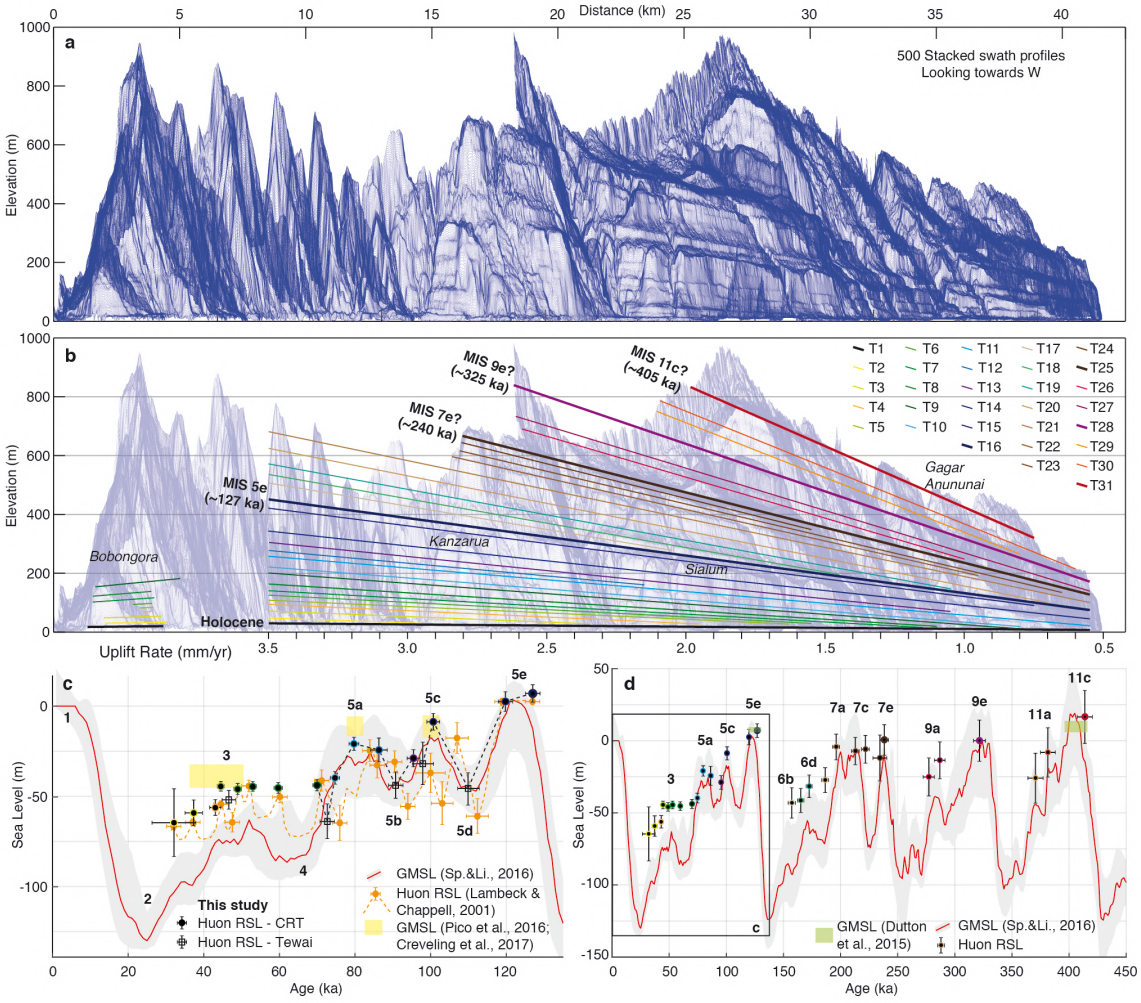

Figure 3: Huon relative sea-level estimates. a) 500 Stacked swath profiles of TanDEM-X Digital Surface Model looking towards the W with **b)** interpretation of coral reef terrace levels **c)** Zoom-in to last glacial-interglacial cycle, with Huon relative sea-level estimates of this study obtained from coral reef terrace geometry in **b** (Huon RSL - CRT; halo colors as in **b**) and perpendicular stacked swath profiles (Supplementary Data 2 and 3; see Methods). We compare these to Huon RSL estimates of Lambeck and Chappell (2001), global mean sea-level estimates of Pico et al., (2016; MIS 3) and Creveling et al., (2017; MIS 5a and 5c), and the global mean sea-level curve of Spratt and Lisiecki (2016) with 97.5% confidence interval (grey band). Lowstand estimates (Huon RSL - Tewai) were re-calculated from Chappell (1983) and Lambeck and Chappell (2001) (see Methods and Supplementary Table 3) **d)** same as **c** but for ~425 ka (halo colors as in **b**), and compared to global mean sea-level estimates of Dutton et al., (2015; MIS 5e, 11c). Marine Isotope Stages (MIS; bold) as defined in Railsback et al. (2015).

and RSL elevation of 7±5 m as a compromise between reasonable MIS 5e minimum and maximum estimates of 2 m (GMSL[3]) and 12 m (GIA-corrected Huon RSL[23]), respectively. Some RSL lowstand elevations were previously calculated from the Tewai section (Fig. 1[14,24]), which we update using our new uplift rate estimates.

New RSL estimates for the last glacial cycle, shown in Fig. 3c, are generally higher in elevation than previous Huon estimates[11]. Our estimates are closer to GIA-corrected GMSL estimates for MIS 3, 5a and 5c interstadials, thus largely accounting for previous discrepancies between Huon and other sites that show higher interstadial sea level[25–27]. In terms of timing, our calculated RSL ages are similar to previous studies for Huon's well-dated MIS 3 and 5e highstands (Fig. 3c), but slightly younger for MIS 5a and 5c highstands, which have not been well-constrained by U-Th dating (Fig. 1d). Instead of ~84 ka (MIS 5a) and ~107 ka (MIS 5c) peak ages[11], we find ages of ~80 ka and ~100 ka, more in line with the peak ages of the GMSL-curve shown in Fig. 3c[4]. Also our re-calculated 5b and 5d lowstands are younger and at higher elevation than previously proposed for Huon[11,14], more in line with the displayed GMSL curve[4] (Fig. 3c). Generally, our proposed terrace ages are in good agreement with dated Huon samples (Supplementary Table 1).

Comparison of our new RSL estimates for the past ~420 ka (Supplementary Table 1) and the GMSL curve of ref[4], as displayed in Fig 3d, shows a remarkable first-order similarity in highstand ages and sea-level elevations. This is especially the case for the interglacial highstands (5e, 7e, 9e, 11c), and we highlight that the similarity of the Huon MIS 11c RSL highstand to independent GMSL estimates[28] lends some support to our assumption that the uplift rate has not changed much over time. More specifically, if our proposed chronology is correct, and we overestimated the age of the MIS 11c peak by ~0-15 ka (difference between ~400-415 ka GMSL highstand age estimate of ref[28], and our ~415 ka RSL estimate; Fig. 3d) that would imply a maximum uplift rate change of 5% between 420-125 ka compared to 125-0 ka. In contrast to interglacial sea-levels, interstadial sea-level highstands (MIS 3, 5a, 5c, 6, 9a, 11a) for Huon seem to be of consistently higher elevation than $\delta^{18}O$-derived GMSL estimates, up to ~20 m for the lower interstadial peaks (Fig. 3d). The offset appears cyclic: larger during lower sea-level and smaller during higher sea-level.

To compare RSL directly with GMSL, it must be corrected for the local effect of glacial isostatic adjustment (GIA). We used GIA modeling (see Methods) with a global ice history characterized by a GMSL history based on the GMSL curve of ref[4]. We found that the GIA correction at this far-field location is less than 7 m, within the uncertainty for most of our RSL estimates (Supplementary Fig. 4). Consequently, our

RSL estimates can be considered to approximate GMSL, and this RSL history constitutes a new key dataset, especially for (>130 ka) interstadials, for which we present some of the first sea-level constraints based on geologic indicators.

Terrace sequence modeling

Different sea-level histories produce distinct coral reef terrace morphologies, as illustrated by numerical models of coral reef terrace sequences[29]. We modelled the Huon coral reef terrace sequence to test 1) whether a full sea-level history with highstands adjusted to our RSL data would reproduce the observed sequence in a direct model and 2) how much the revised RSL estimates would impact the geomorphic architecture of the sequence. We chose three representative cross-sections (Fig. 4) and used the REEF code (updated from refs[30,31]). We test the impact of our RSL estimates by considering 3 different sea-level curves (Fig. 4a; Supplementary Fig. 5): 1) the GMSL-curve of ref[4], 2) a modified version of this curve with the whole curve adjusted upwards to match our RSL highstand estimates 3) a similarly modified curve but with the lowstands fixed. To a first order, the model outputs show that our proposed chronology and uplift rates produce reasonable terrace shapes in comparison to the observed sections (Fig. 4b-d). In the model outputs, major highstands (MIS 5e, 7e, 9e, 11c) produce wider terraces than interstadial terraces, a pattern similar to the observed morphology. All dated samples at the Sialum and Kanzarua sections fit with the modeled reef ages. Checking in more detail, two relevant model results stand out: 1) the Sialum model shows how the 119.3 ka sample just below T14 can have an age corresponding to MIS 5e (Fig. 4c), even if the terrace itself is younger (MIS 5c), and 2) The models also show how multiple terraces can result from a single MIS 5e RSL peak (as in ref[32]), and how the same terrace could have been constructed during multiple times, as observed in the data with clusters of ages around ~115 ka and ~130 ka on the same terrace[19,33,34].

Considering the misfits between modeled and observed terrace elevations, curves with adjusted highstands better fit the observed terrace morphology, particularly for interstadial terraces T11, T14, T20, T25, T27, T29 and T30 in Fig. 4b, T7, T14, T20, T25, T27 and T29 in Fig. 4c, as well as T7, T11, T14 and T20 in Fig. 4d. Differences between the two highstand-adjusted curves are subtle, and preclude a clear preference. Perhaps in future work on finer scale, checking the morphology on m-scale and ages on ka-scale, and incorporating detailed morpho-stratigraphy[16], Huon lowstands can be constrained using reef modeling.

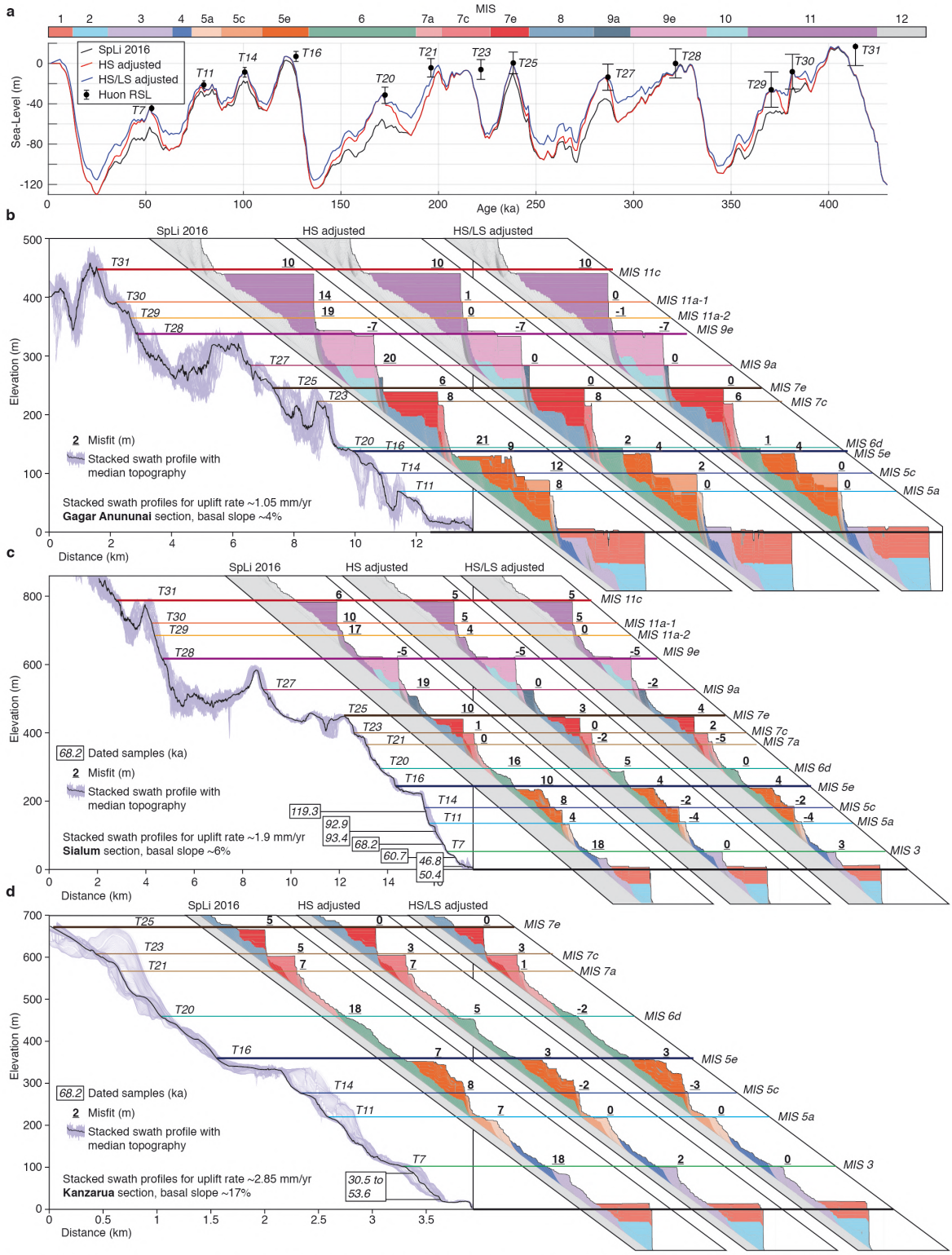

Figure 4: Huon terrace sequence modelling. a) Sea-level curves used for terrace modelling, including the Spratt and Lisiecki (2016) GMSL curve (black), a modified version of that curve with only the highstands (HS) adjusted (red) and a modified version with both high- and lowstands (HS/LS) adjusted (blue). Corrections were only applied for the shown RSL estimates: given the limited number of peaks in the GMSL-curve we only picked the highest Huon RSL estimate per MIS to calibrate. **b)** Modeling results for the Gagar Anununai, **c)** Sialum and **d)** Kanzarua sections, using a potential reef growth rate of 10 mm/yr, erosional potential of 30 mm/yr and basal slopes derived from average topography. Misfits are calculated by subtracting the modeled from the observed terrace elevation, for the terraces labeled in a. Location of stacked swath profiles, derived from the Pleiades DSM, are given in Fig. 1. The dated samples for the Sialum section were taken within the area of the stacked swath profile (Cutler et al., 2003), whereas the dated samples for the Kanzarua section (Chappell et al., 1996; Yokoyama et al., 2001; Cutler et al., 2003) were taken from a location ~2 km S of the stacked swath profile.

We also used reef modelling to test two possible limitations that may have affected our RSL estimates. The first possible limitation is that the actual age of construction of a terrace surface may slightly precede sea-level highstands, and change with uplift rate, as was evidenced for the Holocene Huon terrace[35] (Supplementary Fig. 6). The second potential limitation is that a terrace surface might form several meters below the peak in sea-level (SL-Terrace$_{DIF}$), depending on the morphology formed during preceding sea-level oscillations or erosion of a barrier reef[31]. We quantified these effects (Supplementary Fig. 6) using the range of uplift rates determined for Huon (0.5-3.5 mm/yr) in a series of models using the same parameters as for the models in Fig. 4 (see Methods). These reef simulations suggest that peak-delays and non-negligible values of SL-Terrace$_{DIF}$ could have lead to misinterpretations in Huon RSL highstand elevation, up to ~10-15 m, and age, up to ~10 ka, for the T31 (MIS 11c) terrace, and that values gradually increase with age. However, as offsets between Huon RSL highstands and $\delta^{18}O$-derived GMSL estimates appear to be cyclic, rather than increasing gradually (Fig. 3d), neither peak-delays nor significant values of SL-Terrace$_{DIF}$ can easily explain the highstand discrepancy for interstadial sea-levels.

Implications for eustatic sea-level variations

Collectively, our geometric analysis, and reef modeling results suggest that $\delta^{18}O$-derived curves systematically underestimate sea-level during interstadial periods. A common argument against using RSL estimates like those in Huon is the possibility of non-constant uplift rates[36,37]. While we cannot exclude this possibility, the cyclic pattern of large discrepancies with interstadial highstands and low discrepancies with interglacial highstands (Fig. 3d; Supplementary Fig. 5) is not easily reconciled with a tectonic periodicity. As such, the simplest explanation for the consistently higher Huon RSL estimates in comparison to $\delta^{18}O$-derived GMSL estimates is that the latter does not appropriately account for reduced ice-sheet extent of interstadial highstands. Combined geologic/paleogeographic observations and GIA analysis suggest that indeed global ice volumes may be smaller than inferred from $\delta^{18}O$ records during MIS 3[26,38–40]. Similar trends may hold for the older interstadials peaks within MIS 6, 9a, 11a. We envision two possibilities, either (1) $\delta^{18}O$ has been incorrectly calibrated to sea-level in previous work, or (2) $\delta^{18}O$ does not fully grasp short-lived changes in the growth and decay of ice sheets to begin with.

Considering option (1) above, ref[41] proposed that $\delta^{18}O$ should be calibrated differently for deglaciations than for glaciations. They performed such a separate calibration with RSL indicators, and this is probably why their interstadial highstand elevations are more similar to the Huon data than most other $\delta^{18}O$-derived GMSL

curves, even though they relied on the previous, lower Huon RSL estimates for the interstadial highstand periods. An updated calibration with a similar technique could reconcile $\delta^{18}O$ with geologic indicators. An alternative explanation for relatively low sea-level estimates in $\delta^{18}O$-derived curves is the possibility that sea-level during the last glacial maximum (LGM), to which most $\delta^{18}O$-derived curves are calibrated, may be generally overestimated[42].

Considering option (2) above, it is possible that rapid (~7 ky periodicity) and high-amplitude (10-15 m) sea-level oscillations are long enough to imprint uplifting landscapes, but too short to be well recorded in $\delta^{18}O$ records, which are often stacked or averaged[4]. Such oscillations have been proposed for MIS 3 in Huon[16,43] in relation to Heinrich events[44], supported by the large number of Huon MIS 3 terraces and derived RSL estimates (Fig. 3). Heinrich events may also exist for older interstadial periods than MIS 3[45], although this has never been directly evidenced by geologic data. We note in our analysis that, similar to T2-T8 for MIS 3, T17-19 seem to represent a ~7 ky periodicity for the MIS 6 interval (Fig. 3d). A detailed morpho-stratigraphic analysis of these possible MIS 6 terraces, in combination with dating and modelling (as in refs[16,43]) may shed more light on the possibility of older Heinrich events.

We envision that our new RSL data from the Huon Peninsula may be a prime basis to accurately constrain Quaternary sea-level and its relation with paleoclimate, ice-sheets and geodynamics, motivating a re-evaluation of interstadial highstands and relations of sea-level and $\delta^{18}O$.

Acknowledgements

We thank the Centre Nationale des Etudes Spatiales (CNES) for the Pleiades imagery, and the German Aerospace Center for TanDEM-X data. We also thank Pascal Lacroix for help with DSM calculation, Laurie Barrier for the stacked swath profile code, Eric Lewin for help with statistics and Thomas Lorscheid for help with the indicative meaning calculator. G.G. acknowledges the CNES for his postdoctoral scholarship that made this study possible, and thanks Robin Lacassin for the initial suggestion to re-visit the Huon terrace sequence with Pleiades topography.

Author contributions

G.G. and L.H. designed the study, G.G. produced the Huon DSM and analysed the terrace deformation with the help of stacked swath profiles provided by D.F.-B. G.G.

calculated RSL highstands and T.P. calculated GIA-corrections. G.G. performed the reef modelling with the help of A.-M.P.. and L.H. G.G. carried out discussions with L.H., A.-M.P., D.C., C.A. and K.P. on best general strategies for coral reef terrace analysis. All authors discussed the results at different stages of the process. G.G. wrote the paper with contributions and edits from all other authors.

Competing interest statement

The authors declare no competing interests.

Data availability

The Pleiades satellite imagery was obtained through the ISIS program of the Centre National d'Etudes Spatiales (CNES, France) under an academic license and is not for open distribution. On request, we'll provide the DSM calculated from this imagery to any academic researcher who gets approval from CNES (contact isis-pleiades@cnes.fr for quoting this paper, and with laurent.husson@univ-grenoble-alpes.fr in copy). The other data that support the findings of this study are available within the publication, referenced studies and/or from the corresponding author on request.

References

1. DeConto, R. M. & Pollard, D. Contribution of Antarctica to past and future sea-level rise. *Nature* **531**, 591–597 (2016).
2. Conrad, C. P. & Husson, L. Influence of dynamic topography on sea level and its rate of change. *Lithosphere* (2009).
3. Murray-Wallace, C. V. & Woodroffe, C. D. *Quaternary Sea-Level Changes: A Global Perspective*. (Cambridge University Press, 2014).
4. Spratt, R. M. & Lisiecki, L. E. A Late Pleistocene sea level stack. *Clim. Past* **12**, 1079 (2016).
5. de Gelder, G. *et al.* How do sea-level curves influence modeled marine terrace sequences? *Quat. Sci. Rev.* **229**, 106132 (2020).
6. Pedoja, K. *et al.* Coastal staircase sequences reflecting sea-level oscillations and tectonic uplift during the Quaternary and Neogene. *Earth-Sci. Rev.* **132**, 13–38 (2014/5).
7. Hibbert, F. D. *et al.* Coral indicators of past sea-level change: A global repository of U-series dated benchmarks. *Quat. Sci. Rev.* **145**, 1–56 (2016).
8. Past Interglacials Working Group of PAGES. Interglacials of the last 800,000 years. *Rev. Geophys.* **54**, 162–219 (2016).

9. Thompson, S. B. & Creveling, J. R. A global database of marine isotope substage 5a and 5c marine terraces and paleoshoreline indicators. *Earth Syst. Sci. Data* **13**, 3467–3490 (2021).
10. Chappell, J. Geology of Coral Terraces, Huon Peninsula, New Guinea: A Study of Quaternary Tectonic Movements and Sea-Level Changes. *GSA Bulletin* **85**, 553–570 (1974).
11. Lambeck, K. & Chappell, J. Sea level change through the last glacial cycle. *Science* **292**, 679–686 (2001).
12. Veeh, H. H. & Chappell, J. Astronomical theory of climatic change: support from new Guinea. *Science* **167**, 862–865 (1970).
13. Bloom, A. L., Broecker, W. S., Chappell, J. M. A., Matthews, R. K. & Mesolella, K. J. Quaternary sea level fluctuations on a tectonic coast: New 230Th234U dates from the Huon Peninsula, New Guinea. *Quat. Res.* **4**, 185–205 (1974).
14. Chappell, J. & Shackleton, N. J. Oxygen isotopes and sea level. *Nature* **324**, 137–140 (1986).
15. Chappell, J. *et al.* Reconciliaion of late Quaternary sea levels derived from coral terraces at Huon Peninsula with deep sea oxygen isotope records. *Earth Planet. Sci. Lett.* **141**, 227–236 (1996).
16. Chappell, J. Sea level changes forced ice breakouts in the Last Glacial cycle: new results from coral terraces. *Quat. Sci. Rev.* **21**, 1229–1240 (2002).
17. Kopp, R. E., Simons, F. J., Mitrovica, J. X., Maloof, A. C. & Oppenheimer, M. Probabilistic assessment of sea level during the last interglacial stage. *Nature* **462**, 863–867 (2009).
18. Rovere, A. *et al.* The analysis of Last Interglacial (MIS 5e) relative sea-level indicators: Reconstructing sea-level in a warmer world. *Earth-Sci. Rev.* **159**, 404–427 (2016).
19. Esat, T. M., McCulloch, M. T., Chappell, J., Pillans, B. & Omura, A. Rapid fluctuations in sea level recorded at huon peninsula during the penultimate deglaciation. *Science* **283**, 197–201 (1999).
20. Armijo, R., Lacassin, R., Coudurier-Curveur, A. & Carrizo, D. Coupled tectonic evolution of Andean orogeny and global climate. *Earth-Sci. Rev.* **143**, 1–35 (2015/4).
21. Fernández‐Blanco, D., Gelder, G., Lacassin, R. & Armijo, R. Geometry of flexural uplift by continental rifting in Corinth, Greece. *Tectonics* (2019) doi:10.1029/2019TC005685.

22. Lajoie, K. R. Coastal tectonics. *Active tectonics* (1986).
23. Creveling, J. R., Mitrovica, J. X., Hay, C. C., Austermann, J. & Kopp, R. E. Revisiting tectonic corrections applied to Pleistocene sea-level highstands. *Quat. Sci. Rev.* **111**, 72–80 (2015).
24. Chappell, J. A revised sea level record for the last 300,000 years from Papua New Guinea. *Search.* **14**, 99–101 (1983).
25. Cabioch, G. & Ayliffe, L. K. Raised Coral Terraces at Malakula, Vanuatu, Southwest Pacific, Indicate High Sea Level During Marine Isotope Stage 3. *Quat. Res.* **56**, 357–365 (2001).
26. Pico, T., Mitrovica, J. X., Ferrier, K. L. & Braun, J. Global ice volume during MIS 3 inferred from a sea-level analysis of sedimentary core records in the Yellow River Delta. *Quat. Sci. Rev.* **152**, 72–79 (2016).
27. Creveling, J. R., Mitrovica, J. X., Clark, P. U., Waelbroeck, C. & Pico, T. Predicted bounds on peak global mean sea level during marine isotope stages 5a and 5c. *Quat. Sci. Rev.* **163**, 193–208 (2017).
28. Dutton, A. *et al.* Sea-level rise due to polar ice-sheet mass loss during past warm periods. *Science* **349**, aaa4019 (2015).
29. Toomey, M., Ashton, A. D. & Taylor Perron, J. Profiles of ocean island coral reefs controlled by sea-level history and carbonate accumulation rates. *Geology* **41**, 731–734 (2013).
30. Husson, L. *et al.* Reef carbonate productivity during quaternary sea level oscillations. *Geochem. Geophys. Geosyst.* **19**, 1148–1164 (2018).
31. Pastier, A.-M. *et al.* Genesis and Architecture of Sequences of Quaternary Coral Reef Terraces: Insights From Numerical Models. *Geochem. Geophys. Geosyst.* **20**, 4248–4272 (2019).
32. Pastier, A.-M., Malatesta, L., Huppert, K. & Chauveau, D. Towards a dynamic approach of sequences of coral reef terraces. in https://doi.org/10.5194/egusphere–egu21–15976 (EGU General Assembly, 2021).
33. Stein, M. *et al.* TIMS U-series dating and stable isotopes of the last interglacial event in Papua New Guinea. *Geochim. Cosmochim. Acta* **57**, 2541–2554 (1993).
34. Cutler, K. B. *et al.* Rapid sea-level fall and deep-ocean temperature change since the last interglacial period. *Earth Planet. Sci. Lett.* **206**, 253–271 (2003).
35. Ota, Y. & Chappell, J. Holocene sea-level rise and coral reef growth on a tectonically rising coast, Huon Peninsula, Papua New Guinea. *Quat. Int.* **55**, 51–59 (1999).

36. Saillard, M. *et al.* Andean coastal uplift and active tectonics in southern Peru: 10Be surface exposure dating of differentially uplifted marine terrace sequences (San Juan de Marcona, ~15.4°S). *Geomorphology* **128**, 178–190 (2011).
37. Walker, R. T. *et al.* Rapid mantle-driven uplift along the Angolan margin in the late Quaternary. *Nat. Geosci.* **9**, 909 (2016).
38. Batchelor, C. L. *et al.* The configuration of Northern Hemisphere ice sheets through the Quaternary. *Nat. Commun.* **10**, 3713 (2019).
39. Dalton, A. S. *et al.* Was the Laurentide Ice Sheet significantly reduced during Marine Isotope Stage 3? *Geology* **47**, 111–114 (2019).
40. Gowan, E. J. *et al.* A new global ice sheet reconstruction for the past 80 000 years. *Nat. Commun.* **12**, 1199 (2021).
41. Waelbroeck, C. *et al.* Sea-level and deep water temperature changes derived from benthic foraminifera isotopic records. *Quat. Sci. Rev.* **21**, 295–305 (2002).
42. Simms, A. R., Lisiecki, L., Gebbie, G., Whitehouse, P. L. & Clark, J. F. Balancing the last glacial maximum (LGM) sea-level budget. *Quat. Sci. Rev.* **205**, 143–153 (2019).
43. Yokoyama, Y., Esat, T. M. & Lambeck, K. Coupled climate and sea-level changes deduced from Huon Peninsula coral terraces of the last ice age. *Earth Planet. Sci. Lett.* **193**, 579–587 (2001).
44. Heinrich, H. Origin and consequences of cyclic ice rafting in the Northeast Atlantic Ocean during the past 130,000 years. *Quat. Res.* **29**, 142–152 (1988).
45. Hodell, D. A., Channell, J. E. T., Curtis, J. H., Romero, O. E. & Röhl, U. Onset of 'Hudson Strait' Heinrich events in the eastern North Atlantic at the end of the middle Pleistocene transition (~640 ka)? *Paleoceanography* **23**, (2008).
46. Abers, G. A. & McCaffrey, R. Active arc-continent collision: Earthquakes, gravity anomalies, and fault kinematics in the Huon-Finisterre collision zone, Papua New Guinea. *Tectonics* **13**, 227–245 (1994).
47. de Gelder, G. *et al.* Corinth terraces re-visited: Improved paleoshoreline determination using Pleiades-DEMs. *Geotectonic Research*. **97**, 12–14 (2015).
48. Railsback, L. B., Gibbard, P. L., Head, M. J., Voarintsoa, N. R. G. & Toucanne, S. An optimized scheme of lettered marine isotope substages for the last 1.0 million years, and the climatostratigraphic nature of isotope stages and substages. *Quat. Sci. Rev.* **111**, 94–106 (2015).

Figure legends

Figure 1: Uplift rates, dated samples and tectonic context of the Huon coral reef terrace sequence. a) Slope map of coral reef terrace sequence overlain with colored elevations, showing a comparison of the uplift rates proposed by ref[10] and this study. We also show the location of dated samples, and shoreline angles for the upper MIS 5e (~127 ka) terrace. Names in italic refer to the locations of commonly studied sections, of which 3 are modeled in Fig. 4. **b)** Regional tectonic setting, with earthquake focal mechanisms of the 1967 and 1992 seismic sequences from ref[46] ranging from m_b = 5.5 (smallest) to 6.2 (largest). **c)** Detailed DSM slope map of the Sialum area, with mapped paleoshorelines for the coral reef terraces. **d)** Ages of dated samples within the compilation of ref[7]. All samples in blue, and in orange the samples after removing duplicates, samples out of the study area and U/Th open system samples.

Figure 2: Best-fitting tilt direction of Huon coral reef terrace sequence. a) Example of shoreline angle determination, at the intersection between terrace and paleo-cliff, using a free-cliff analysis[47]. Black line marks the maximum elevation of the swath profile in Fig. 1c. The orange and blue lines represent a minimum and maximum approximation, respectively, to derive the shoreline angle elevation. **b)** Linear surface fitting of MIS 5e shoreline angle elevations (blue dots), using the average values of the minima and maxima derived as in **a**. Results indicate a simple planar tilt approximately N-ward (N002E) **c)** Histogram of residuals of surface fitting including standard deviation (STD), with distribution not significantly different from Gaussian at 95% confidence as suggested by a X^2 test.

Figure 3: Huon relative sea-level estimates. a) 500 Stacked swath profiles of TanDEM-X Digital Surface Model looking towards the W with **b)** interpretation of coral reef terrace levels **c)** Zoom-in to last glacial-interglacial cycle, with Huon relative sea-level estimates of this study obtained from coral reef terrace geometry in **b** (Huon RSL - CRT; halo colors as in **b**) and perpendicular stacked swath profiles (Supplementary Data 2 and 3; see Methods). We compare these to Huon RSL estimates of ref[11], global mean sea-level estimates of ref[26] (MIS 3) and ref[27] (MIS 5a and 5c), and the global mean sea-level curve of ref[4] with 97.5% confidence interval (grey band). Lowstand estimates (Huon RSL - Tewai) were re-calculated from ref[24] and ref[11] (see Methods and Supplementary Table 3) **d)** same as **c** but for ~425 ka

(halo colors as in **b**), and compared to global mean sea-level estimates of ref[28] (MIS 5e, 11c). Marine Isotope Stages (MIS; bold) as defined in ref[48].

Figure 4: Huon terrace sequence modelling. **a)** Sea-level curves used for terrace modelling, including the ref[4] GMSL curve (black), a modified version of that curve with only the highstands (HS) adjusted (red) and a modified version with both high- and lowstands (HS/LS) adjusted (blue). Corrections were only applied for the shown RSL estimates: given the limited number of peaks in the GMSL-curve we only picked the highest Huon RSL estimate per MIS to calibrate. **b)** Modeling results for the Gagar Anununai, **c)** Sialum and **d)** Kanzarua sections, using a potential reef growth rate of 10 mm/yr, erosional potential of 30 mm/yr and basal slopes derived from average topography. Misfits are calculated by subtracting the modeled from the observed terrace elevation for the terraces labeled in **a**. Location of stacked swath profiles, derived from the Pleiades DSM, are given in Fig. 1. The dated samples for the Sialum section were taken within the area of the stacked swath profile[34], whereas the dated samples for the Kanzarua section[15,34,43] were taken from a location ~2 km S of the stacked swath profile.

Methods

Digital Surface Model (DSM) calculation

We used tri-stereo 0.5 m-resolution Pleiades satellite images to calculate the topography of the Huon Peninsula terrace sequence. The open-source software Ames Stereopipeline[49] allowed us to produce ortho-rectified images, point clouds and a 2 m-resolution DSM, to which we applied a -58.9 m vertical correction to account for the geoid height. We ground-checked absolute elevations of 10 control points along the coastline, that were all between 0 and 1 m elevation. We used 12 m-resolution TanDEM-X topography to fill in the gaps that resulted from cloud coverage within the Pleiades DSM, and a 30 m-resolution ALOS DSM for remaining gaps.

Terrace tilt

We calculated large-scale parallel swath profiles with Topotoolbox 2.0[50] and stacked them orthogonal to their trend using an in-house script. This wide swath[20], later termed stacked swaths[21], is a 2D profile of hundreds of narrow-width topographic swath profiles plot together as thin-air lines. Stacked swaths highlight the coherence of the topography along the point of view, i.e. in depth, and the consistency in slope and overall morphology of the topography perpendicular to the point of view. We find the view of the topography that is most coherent regarding the tilt of the terrace sequence, i.e. that perpendicular to the tilt (Supplementary Fig. 1), using the average topography of swath profiles on the TanDEM-X DSM and several viewing angles. The width of each swath profile is computed dynamically, as the total width of the data in the viewpoint direction divided by the chosen number of swaths. We secure an average swath profile width of ~50 m, regardless of viewing angle, plotting a variable number (between 400 and 700) of swath profiles.

Terrace deformation

We followed the detailed mapping of the Sialum section in ref[33] and age interpretations of ref[19] to locate the continuous MIS 5a and 5e terraces on the DSM. From this location, we continued mapping paleoshorelines of these terrace levels NW and SE ward along the coastline. For this, we used a combination of satellite imagery, slope maps and hillshade images of the DSM. We derived shoreline angles by systematically placing ~350 cliff-perpendicular swath profiles along the inner edges of the MIS 5a and 5e terraces, using TerraceM[51] (to Supplementary Fig. 2). To reduce the influence of gravitational, karstic and/or fluvial erosion we used the maximum topography of 100 m-wide swath profiles (as in ref[52]). Assuming a broad range of 60-90° as paleocliff slope, we used a free-cliff analysis[47] to calculate

minimum and maximum shoreline angle elevations by picking a most seaward/landward position of the paleo-seacliff, respectively (Fig. 2a; Supplementary Data 1). The shoreline angles plotted in Figs. 1 and 2 are the average values between minimum and maximum calculated positions. We used a linear surface fitting function to constrain the deformation pattern, assuming a simple, linear tilt, for both the MIS 5a and 5e shoreline angles (Fig. 2; Supplementary Fig. 3). We performed critical χ2 tests to confirm that the residuals follow a Gaussian distribution and the shoreline angle dataset is well described by a linear surface, which was the case for both the MIS 5a and 5e shoreline angles (Fig. 2; Supplementary Fig. 3).

RSL highstand calculation

Coral reef terraces in Huon were previously described with Latin numerals and subdivisions[10]. Given that we do not have direct observations of the internal reef structure, we opted for a simpler designation of terrace numbers (T1-T31; Fig. 3; Supplementary Table 1). To calculate uplift rates, *U*, we used the shoreline angle elevations of T16 (MIS 5e), as follows:

$$U = \frac{H_{SA} - H_{RSL} + H_{REF}}{T} \quad \text{[Formula 1]}$$

where H_{SA} is the shoreline angle elevation, H_{RSL} the relative sea-level elevation with respect to present-day sea-level, H_{REF} the average reference water level for Huon coral reef terraces and T the time of terrace formation. To calculate standard errors we used:

$$\sigma_U{}^2 = U^2 \left(\left(\frac{\sigma_{H_{SA}}{}^2 + \sigma_{H_{RSL}}{}^2 + \sigma_{H_{REF}}{}^2 + \sigma_{H_{SEIS}}{}^2 + \sigma_{H_{DSM}}{}^2}{(H_{SA} - H_{RSL} + H_{REF})^2} \right) + \left(\frac{\sigma_T{}^2}{T^2} \right) \right) \quad \text{[Formula 2]}$$

where σ_{HSA}, σ_{HRSL}, σ_{HREF}, σ_{HSEIS}, σ_{HDSM} and σ_T are the uncertainties in shoreline angle elevation, RSL, reference water level, seismic cycle influence, DSM elevation and time of terrace formation, respectively. We calculated σ_{HSA} by dividing the difference between the maximum and minimum shoreline angle estimates by two. For H_{RSL} and σ_{HRSL} we use 7±5 m here, as a compromise between reasonable MIS 5e minimum and maximum estimates of 2 m[3] and 12 m[23], respectively. For H_{REF} and σ_{HREF} we use 0.66±0.33 m, as calculated with the indicative meaning calculator[53] (Supplementary Table 2). For σ_{HSEIS} we used the results of ref[54] on the Holocene seismic cycles, who found that at any given moment the short-term uplift was within ±1.5 m of the long-term expected uplift at a site with long-term averaged ~3 mm/yr uplift rate. Assuming that long-term uplift is a cumulative effect of several seismic cycles[55], and thus the long-term uplift rate is proportional to the seismic cycle deviation, we use $\sigma_{HSEIS} = U/2$ as a rough estimation. For σ_{HDSM} we use a value of 1 m, which is a conservative

estimate given that other studies using the same calculation method with Pleiades satellite images found DSM standard errors of 0.3-0.5 m[56–58]. For T and σ_T we use 127±2 ka for MIS 5e, as was used in ref[11] following careful assessment of dated samples.

We express the uplift rate as a linear function of latitude l in meters to propose highstand ages and elevations for the non-dated terraces. Following our deformation assessment, we used a weighted fit of the shoreline-angle derived uplift rate estimates in the form $U = A + Bl$. Following ref[59], we introduced the weights $w = 1/\sigma_U^2$, with best estimates for constants A and B calculated from:

$$A = \frac{\sum wl^2 \sum wU - \sum wl \sum wlU}{\Delta} \quad \text{[Formula 3]}$$

$$B = \frac{\sum w \sum wlU - \sum wl \sum wU}{\Delta} \quad \text{[Formula 4]}$$

with

$$\Delta = \sum w \sum wl^2 - (\sum wl)^2 \quad \text{[Formula 5]}$$

And the uncertainties in A and B as:

$$\sigma_A = \sqrt{\frac{\sum wl^2}{\Delta}} \quad \text{[Formula 6]}$$

$$\sigma_B = \sqrt{\frac{\sum w}{\Delta}} \quad \text{[Formula 7]}$$

We used the calculated relation between U and l to estimate the latitude (given a strict northward tilt) for which U = 0 mm/yr, and subsequently to estimate RSL highstand elevations and ages for the other coral reef terraces. We quantified shoreline angle elevations for all terraces from E-W oriented, 2 m resolution stacked swath profiles (Supplementary Data 2), with widths of ~700 m corresponding to uplift rate steps of approximately 0.05 mm/yr (Supplementary Fig. 2). We then added H_{REF} of 0.66 m to every shoreline angle estimate to obtain past sea-level elevations SL_P, with a standard error calculated from σ_{HSA}, σ_{HREF}, σ_{HSEIS} and σ_{HDSM}. Using Formulas 3-7, but replacing U with SL_P, we obtained a linear weighted fit of the corrected shoreline angles for every terrace (Supplementary Data 3). We estimate the age of each terrace, using pure proportionality:

$$\mathrm{T}_{TER} = T_{T16} \cdot \frac{B_{TER}}{B_{T16}} \quad \text{[Formula 8]}$$

with standard error

$$\sigma_{T_{TER}} = T_{TER} \cdot \sqrt{(\frac{\sigma_{T_{T16}}}{T_{T16}})^2 + (\frac{\sigma_{B_{TER}}}{B_{TER}})^2 + (\frac{\sigma_{B_{T16}}}{B_{T16}})^2} \quad \text{[Formula 9]}$$

Where T_{T16}, B_{T16} and its corresponding standard errors are age and slope, respectively, from the T16 (MIS 5e) terrace. To estimate the RSL elevation for each terrace, we used

$$\mathrm{H}_{RSL} = A_{TER} + (B_{TER} \cdot l_{u=0}) \quad \text{[Formula 10]}$$

with standard error

$$\sigma_{H_{RSL}} = \sqrt{\sigma_{A_{TER}}{}^2 + (B_{TER} \cdot l_{u=0} \cdot \sqrt{(\frac{\sigma_{B_{TER}}}{B_{TER}})^2 + (\frac{\sigma_{l_{u=0}}}{l_{u=0}})^2})^2} \quad \text{[Formula 11]}$$

In which A_{TER} and B_{TER} are constants to fit each terrace. Finally, to re-calculate the lowstand elevations given in previous work[11,14,24] we considered the elevations of delta deposits in the Tewai section (Fig. 1), but we used our new uplift rate estimates instead of previously used uplift rates of 3.3-3.5 mm/yr (Supplementary Table 3). We use the same age and elevation uncertainties as previously given to these lowstands, and as previously done, place our best guess for the age in the middle between the preceding and following highstands.

GIA calculation

To calculate relative sea-level change at the Huon Peninsula, we used a gravitationally self-consistent glacial isostatic adjustment model. Our calculations are based on the theory and pseudo-spectral algorithm described by ref[60] with a spherical harmonic truncation at degree and order 512. These calculations solve the full sea-level equation, including the impact of load-induced Earth rotation changes on sea level[61,62], evolving shorelines and the migration of grounded portions of marine-based ice sheets[60,63–65].

Our numerical predictions required models for Earth's viscoelastic structure and the history of global ice cover. We adopted the viscosity profile VM2[66], and tested the sensitivity to this choice by running two simulations using earth models characterized by (1) a lithospheric thickness of 71 km, an upper and lower mantle viscosity of $3\text{x}10^{20}$ Pa · s, and $5\text{x}10^{21}$ Pa s, respectively, and (2) a lithospheric thickness of 48 km, an upper and lower mantle viscosity of $5\text{x}10^{20}$ Pa s, and $15\text{x}10^{21}$ Pa · s, respectively. These earth structure parameters are in agreement with the range estimated in ref[11]. We created a global ice sheet history associated with the GMSL history inferred in ref[4]. We modified the GMSL curves to include no excess melting during interglacials. For GMSL values greater than zero, we assigned the present-day ice sheet geometry

with a GMSL value of zero. We constructed this ice history by assuming that ice geometry in the pre-LGM period is identical to the time in the post-LGM period with the same GMSL value, using the deglacial ice sheet reconstruction in ICE-5G[66]. Our glacial isostatic adjustment calculations were performed for ice sheet loading changes at increments of 2 ky from 430 ka to 32 ka, increments of 1 ky from 32 ka to 17 ka, and increments of 0.5 ka from 17 ka to 0 ka (similar time steps to ICE-5G).

Terrace sequence modelling

We used shape-preserving spline interpolations to calculate the adjusted sea-level curves (Supplementary Fig. 5), modified from the GMSL-curve of ref[4]. For the highstand-adjusted curve we used the difference between our calculated RSL highstands and the GMSL highstands, and values of 0-m for lowstands, whereas for the high- and lowstand adjusted curves we left out the 0-m values for lowstands (Supplementary Fig. 5). The MIS peaks for which we have multiple RSL estimates, we picked the highest RSL estimate to adjust to the GMSL-curve of ref[4]. For the reef modeling, we used a potential reef growth rate of 10 mm/yr, as was used in ref[16] based on U-series dating of the Late-Glacial reef[67]. We used a basal slope similar to the average slope along the modeled profiles, and erosional potential of 30 mm/yr (see full description of the parameterization in ref[31]).

We did a series of modelling tests using the highstand adjusted sea-level curve to check the possible effects of sea-level peak-delays and coral reef terraces forming several meters below sea-level (SL-Terrace$_{DIF}$; Supplementary Fig. 6). As for Fig. 4, we modelled terrace sequences for an uplift rate range of 0.5-3.5 mm/yr, potential reef growth rate of 10 mm/yr, erosional potential of 30 mm/yr and basal slopes similar to Huon stacked swath profiles (Supplementary Data 2). To constrain the peak-delays, we checked the ages at which the shoreline angles of the different coral reef terraces formed, and the difference between the peak in sea-level of the corresponding highstand (Supplementary Fig. 6a, c). To constrain SL-Terrace$_{DIF}$, we checked the difference between the theoretical elevation of the coral reef terrace and the elevation at which the terrace formed (Supplementary Fig. 6b, d). Following the same approach as in the previous section (RSL highstand calculation; Fig. 2), we then calculated RSL highstands from the morphology of the coral reef terrace sequence, to compare with the RSL curve used as model input. This allowed us to have a rough estimate of how much peak-delays and SL-Terrace$_{DIF}$ could have influenced our Huon RSL estimates (Supplementary Fig. 6e).

References Methods

49. Beyer, R. A., Alexandrov, O. & McMichael, S. The Ames stereo pipeline: NASA's open source software for deriving and processing terrain data. *Earth Space Sci.* **5**, 537–548 (2018).

50. Schwanghart, W. & Scherler, D. TopoToolbox 2--MATLAB-based software for topographic analysis and modeling in Earth surface sciences. *Earth Surface Dynamics* **2**, 1–7 (2014).

51. Jara-Muñoz, J., Melnick, D., Pedoja, K. & Strecker, M. R. TerraceM-2: A Matlab® interface for mapping and modelling marine and lacustrine terraces. *Front Earth Sci. Chin.* **7**, 255 (2019).

52. Jara-Muñoz, J., Melnick, D. & Strecker, M. R. TerraceM: A MATLAB® tool to analyze marine and lacustrine terraces using high-resolution topography. *Geosphere* **12**, 176–195 (2016).

53. Lorscheid, T. & Rovere, A. The indicative meaning calculator--quantification of paleo sea-level relationships by using global wave and tide datasets. *Open Geospatial Data, Software and Standards* **4**, 10 (2019).

54. Ota, Y. & Chappell, J. Late Quaternary coseismic uplift events on the Huon Peninsula, Papua New Guinea, deduced from coral terrace data. *J. Geophys. Res.* **101**, 6071–6082 (1996).

55. King, G. C. P., Stein, R. S. & Rundle, J. B. The Growth of Geological Structures by Repeated Earthquakes 1. Conceptual Framework. *J. Geophys. Res.* **93**, 13307–13318 (1988).

56. Zhou, Y., Parsons, B., Elliott, J. R., Barisin, I. & Walker, R. T. Assessing the ability of Pleiades stereo imagery to determine height changes in earthquakes: A case study for the El Mayor‐Cucapah epicentral area. *J. Geophys. Res. [Solid Earth]* **120**, 8793–8808 (2015).

57. Bagnardi, M., González, P. J. & Hooper, A. High-resolution digital elevation model from tri-stereo Pleiades-1 satellite imagery for lava flow volume estimates at Fogo Volcano. *Geophys. Res. Lett.* **43**, 6267–6275 (2016).

58. Almeida, L. P. *et al.* Deriving High Spatial-Resolution Coastal Topography From Sub-meter Satellite Stereo Imagery. *Remote Sensing* **11**, 590 (2019).

59. Taylor, J. *Introduction to Error Analysis, the Study of Uncertainties in Physical Measurements, 2nd Edition*. (ui.adsabs.harvard.edu, 1997).

60. Kendall, R. A., Mitrovica, J. X. & Milne, G. A. On post-glacial sea level--II. Numerical formulation and comparative results on spherically symmetric models. *Geophys. J. Int.* **161**, 679–706 (2005).

61. Milne, G. A. & Mitrovica, J. X. Postglacial sea-level change on a rotating Earth: first results from a gravitationally self-consistent sea-level equation. *Geophys. J. Int.* **126**, F13–F20 (1996).
62. Mitrovica, J. X., Wahr, J., Matsuyama, I. & Paulson, A. The rotational stability of an ice-age earth. *Geophys. J. Int.* **161**, 491–506 (2005).
63. Johnston, P. The effect of spatially non-uniform water loads on prediction of sea-level change. *Geophys. J. Int.* **114**, 615–634 (1993).
64. Milne, G. A., Mitrovica, J. X. & Davis, J. L. Near-field hydro-isostasy: the implementation of a revised sea-level equation. *Geophys. J. Int.* **139**, 464–482 (1999).
65. Lambeck, K., Purcell, A., Johnston, P., Nakada, M. & Yokoyama, Y. Water-load definition in the glacio-hydro-isostatic sea-level equation. *Quat. Sci. Rev.* **22**, 309–318 (2003).
66. Peltier, W. R. & Fairbanks, R. G. Global glacial ice volume and Last Glacial Maximum duration from an extended Barbados sea level record. *Quat. Sci. Rev.* **25**, 3322–3337 (2006).
67. Edwards, R. L. *et al.* A Large Drop in Atmospheric 14C/12C and Reduced Melting in the Younger Dryas, Documented with 230Th Ages of Corals. *Science* **260**, 962–968 (1993).

Supplementary Information

High interstadial sea levels over the past 420ka from Huon terraces (Papua New Guinea)

Gino de Gelder[1*], Laurent Husson[1], Anne-Morwenn Pastier[2], David Fernández-Blanco[3], Tamara Pico[4], Denovan Chauveau[5], Christine Authemayou[5], Kevin Pedoja[6]

1) ISTerre, Université Grenoble-Alpes, Grenoble, France, 2) Geo Forschungs Zentrum, Potsdam, Germany, 3) Barcelona Center for Subsurface Imaging, Barcelona, Spain, 4) California Institute of Technology, Pasadena, US, 5) Université de Bretagne Occidentale, Brest, France, 6) Université de Caen, Caen, France

* Corresponding author: gino.de-gelder@univ-grenoble-alpes.fr

This file includes 6 Supplementary Figures, 3 Supplementary Tables and 3 Supplementary Datasets. The Supplementary Data can be retrieved with these links:

Supplementary Data 1 : https://doi.org/10.6084/m9.figshare.15028923

Supplementary Data 2 : https://doi.org/10.6084/m9.figshare.15028953

Supplementary Data 3 : https://doi.org/10.6084/m9.figshare.15028992

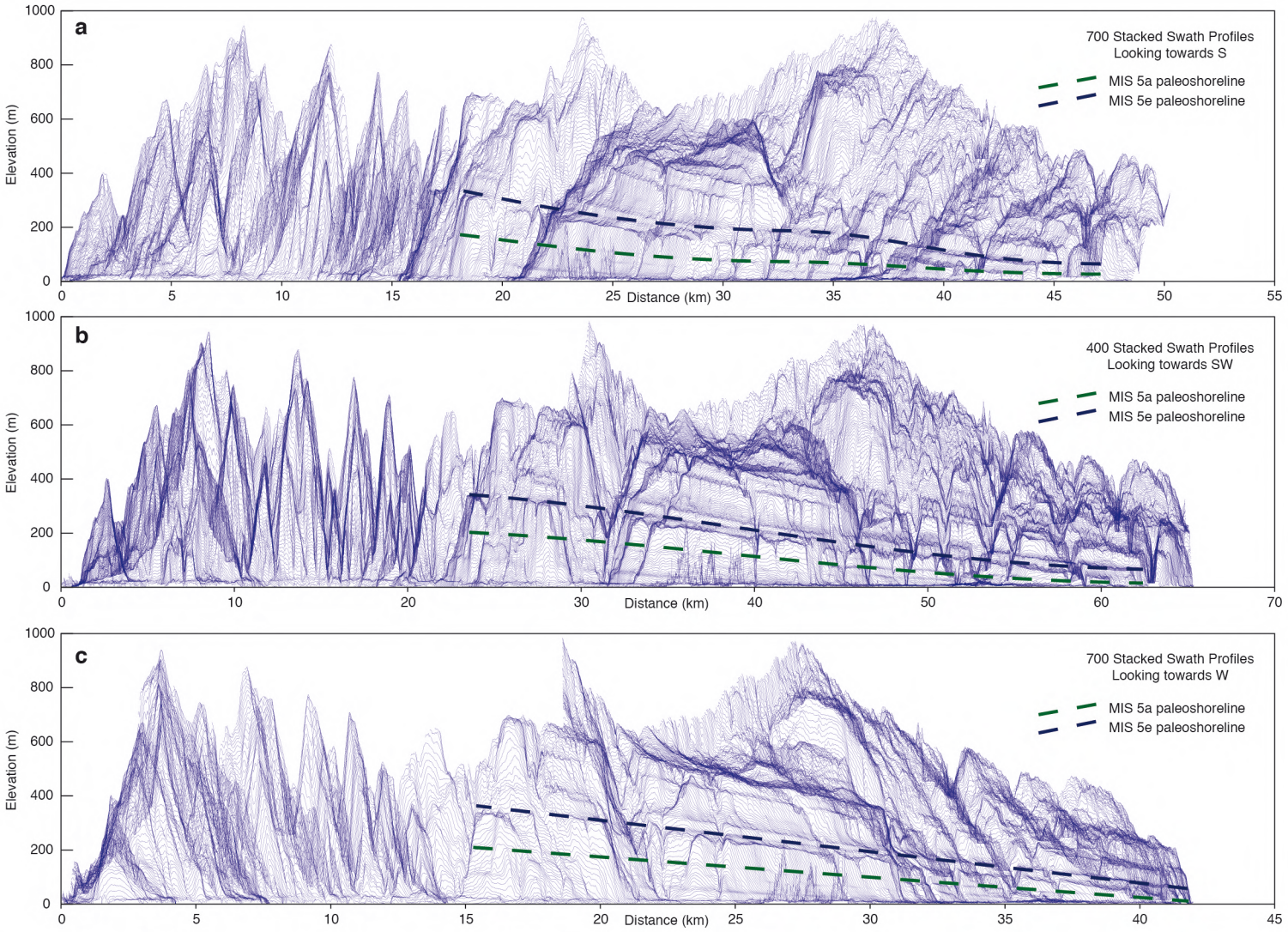

Supplementary Fig. 1: Stacked swath profile views from different directions. Stacked swath profile projections (Armijo et al., 2015) of TanDEM-X Digital Surface Model looking towards the S (**a**), SW (**b**) and W (**c**), with MIS 5a and 5e paleoshorelines marked in green and blue, respectively. If the sequence is tilted, terraces would appear as straight lines when plotted across strike; the stacked swaths along different viewing directions thus suggest that the simplest approximation of the deformation pattern is a N-ward directed tilt.

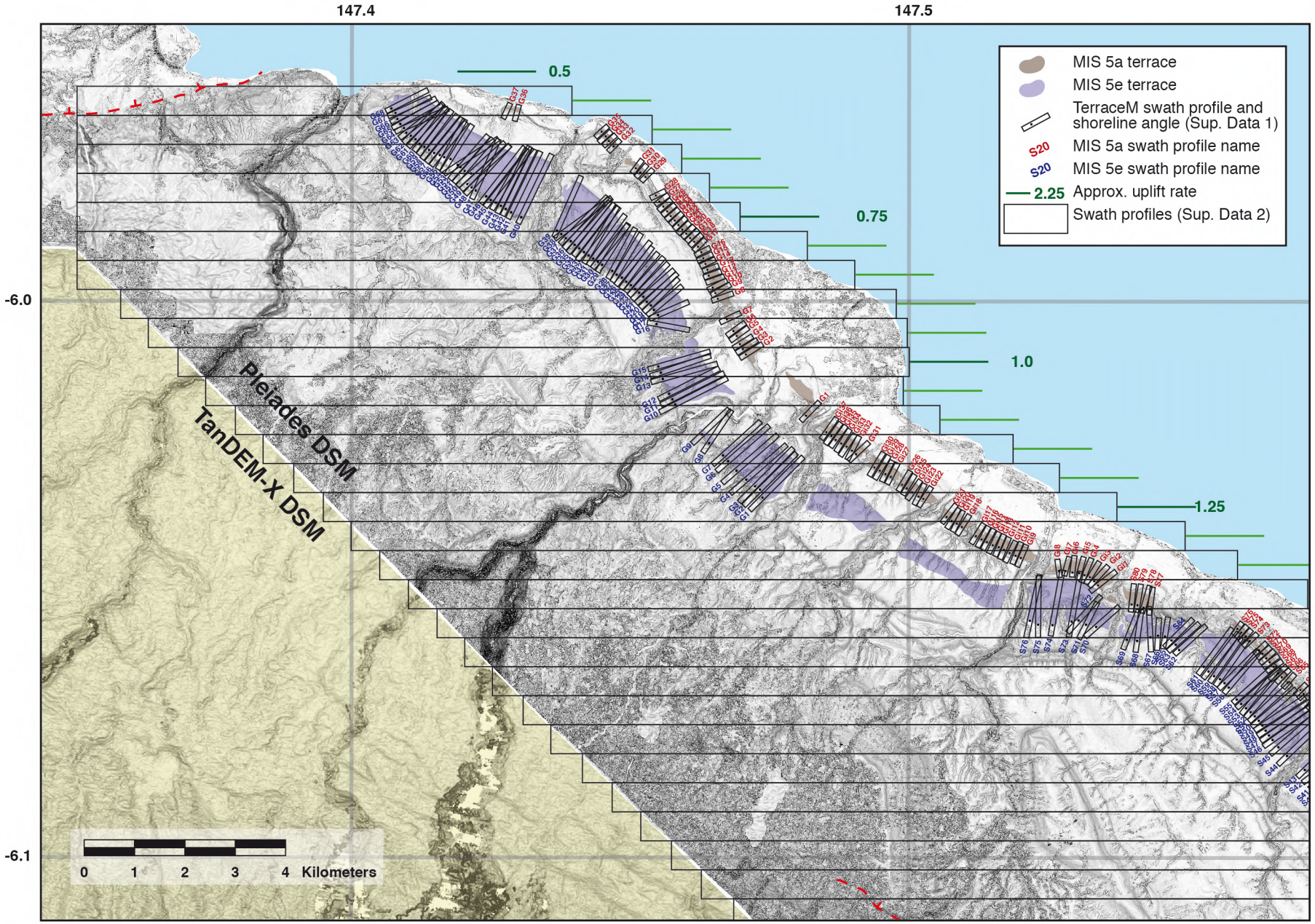
147.4
147.5
-6.0
-6.1
0.5
0.75
1.0
1.25
MIS 5a terrace
MIS 5e terrace
TerraceM swath profile and shoreline angle (Sup. Data 1)
S20 MIS 5a swath profile name
S20 MIS 5e swath profile name
2.25 Approx. uplift rate
Swath profiles (Sup. Data 2)
Pleiades DSM
TanDEM-X DSM
0 1 2 3 4 Kilometers

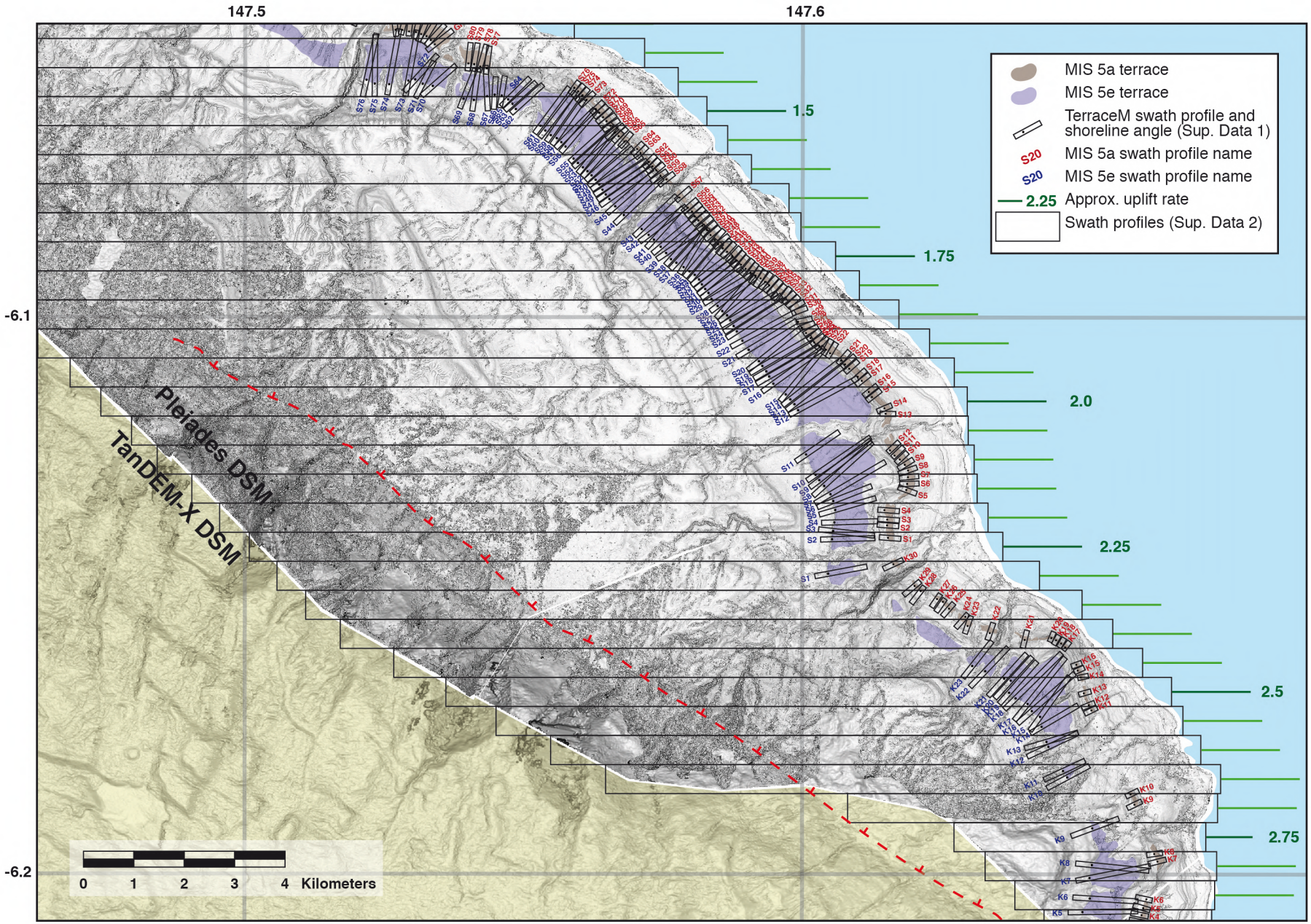
147.5
147.6
-6.1
-6.2
MIS 5a terrace
MIS 5e terrace
TerraceM swath profile and shoreline angle (Sup. Data 1)
S20 MIS 5a swath profile name
S20 MIS 5e swath profile name
2.25 Approx. uplift rate
Swath profiles (Sup. Data 2)
1.5
1.75
2.0
2.25
2.5
2.75
Pleiades DSM
TanDEM-X DSM
0 1 2 3 4 Kilometers

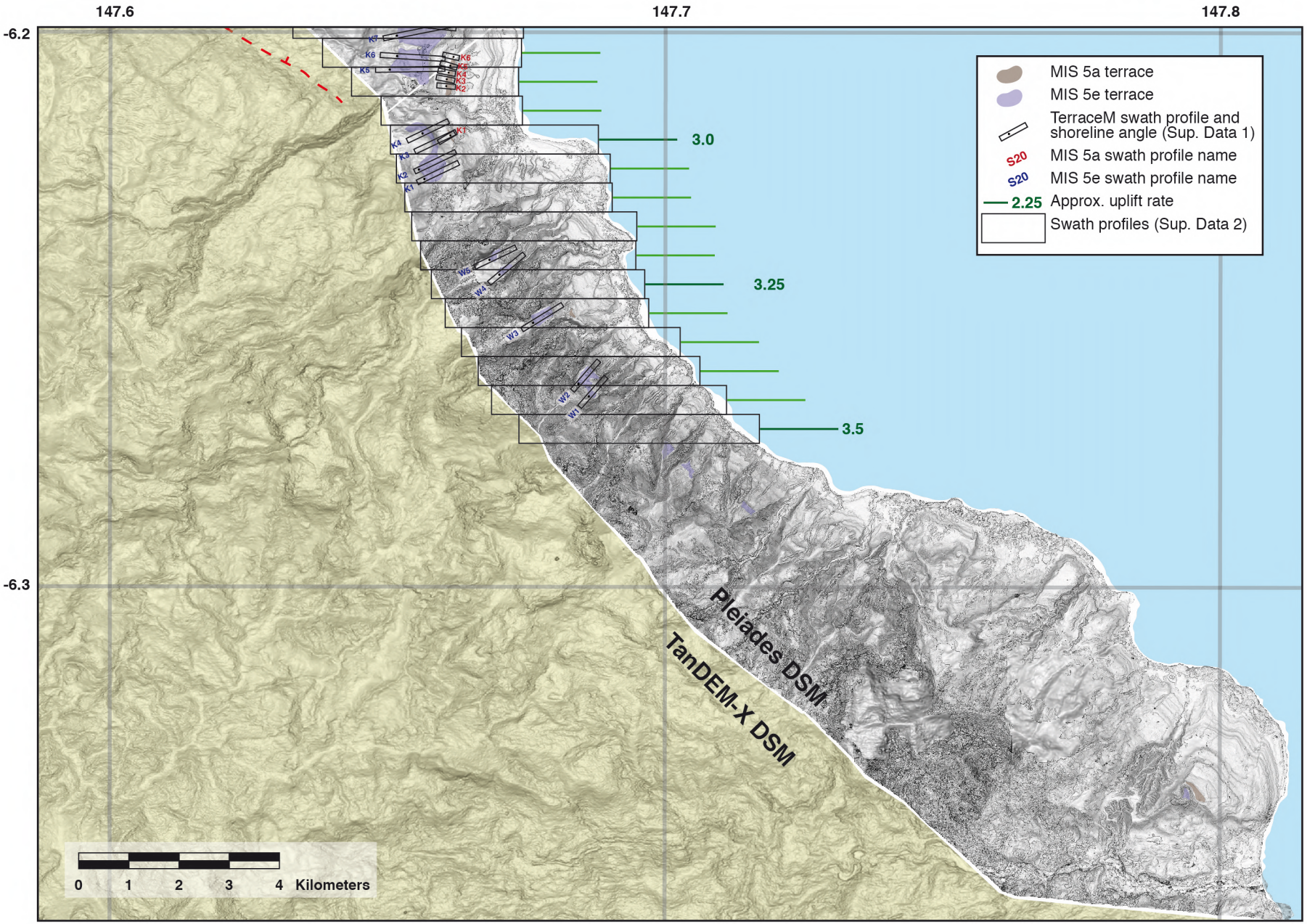

Supplementary Fig. 2: TerraceM swath profile locations. Slope maps of NW **(a),** central **(b)** and SE **(c)** area of the Huon coral reef terrace sequence, showing mapped MIS 5a (red) and MIS 5e (blue) terraces, as well as locations of swath profiles for TerraceM shoreline angle analysis (see methods) and large swath profiles (Supplementary Data 2). W=Wandokai, K=Kanomi, S=Sialum, Gi=Gitukia, G=Gagar Anununai

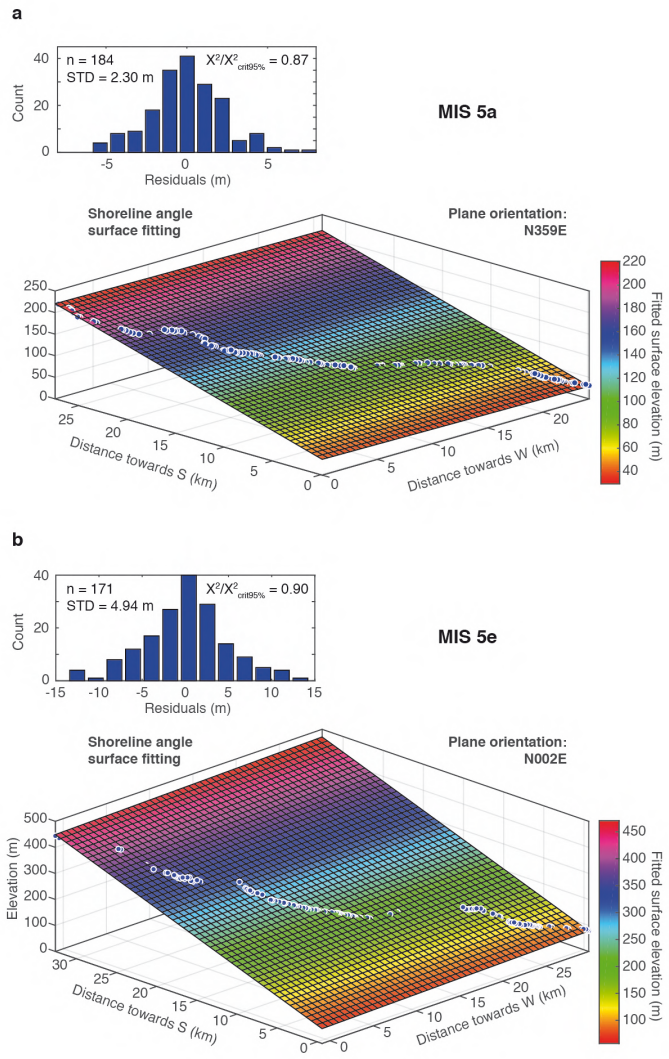

Supplementary Fig. 3: Linear surface fitting of shoreline angles. Surface fitting for **a)** MIS 5a and **b)** MIS 5e shoreline angles (same as in Fig. 2). Histogram shows residuals of surface fitting including standard deviation (STD), with distribution not significantly different from Gaussian at 95% confidence as suggested by an X2 test.

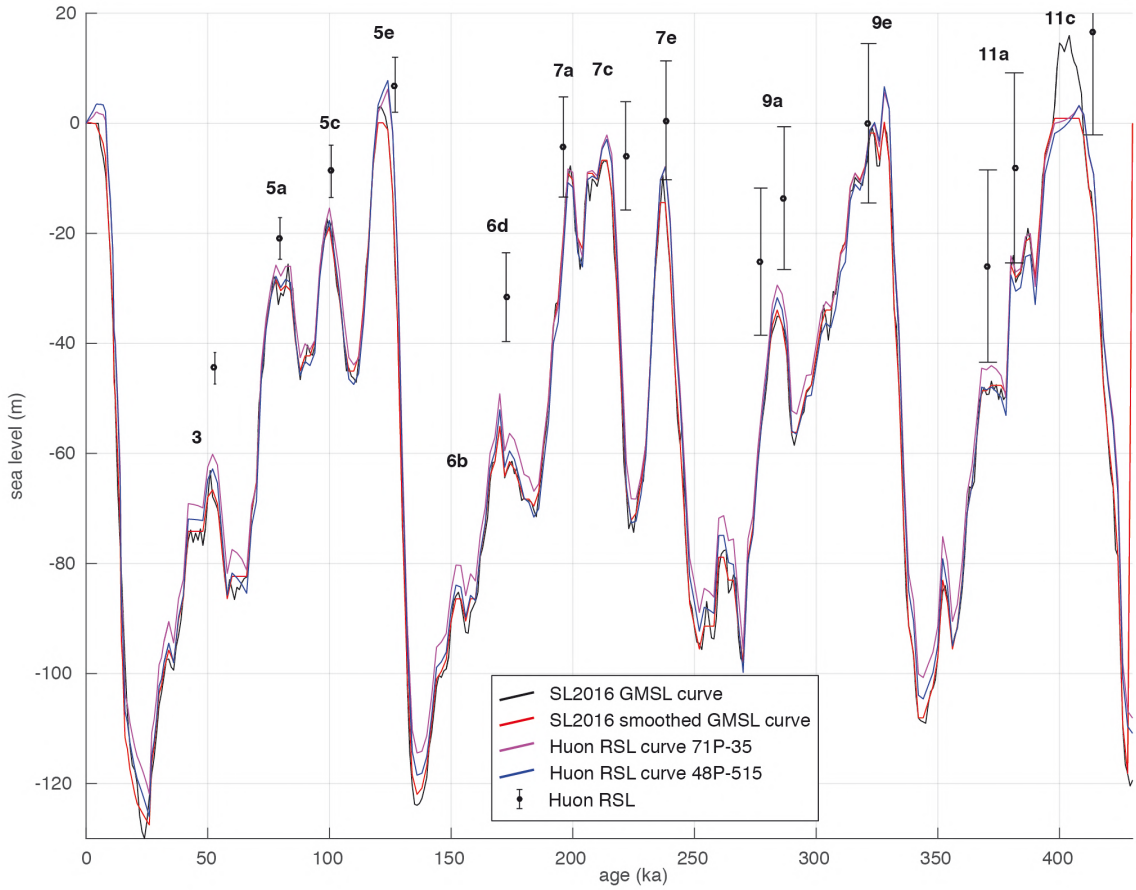

Supplementary Fig. 4: Glacio-Isostatic Adjustment corrected sea-level. Global Mean Sea Level estimates of Spratt and Lisiecki 2016 (black), a downsampled version of that curve (red), and two Huon relative sea-level curves (purple and blue) calculated from the global ice history associated with the downsampled GMSL curve with two different earth models (see methods). Marine Isotope Stages are labeled in bold.

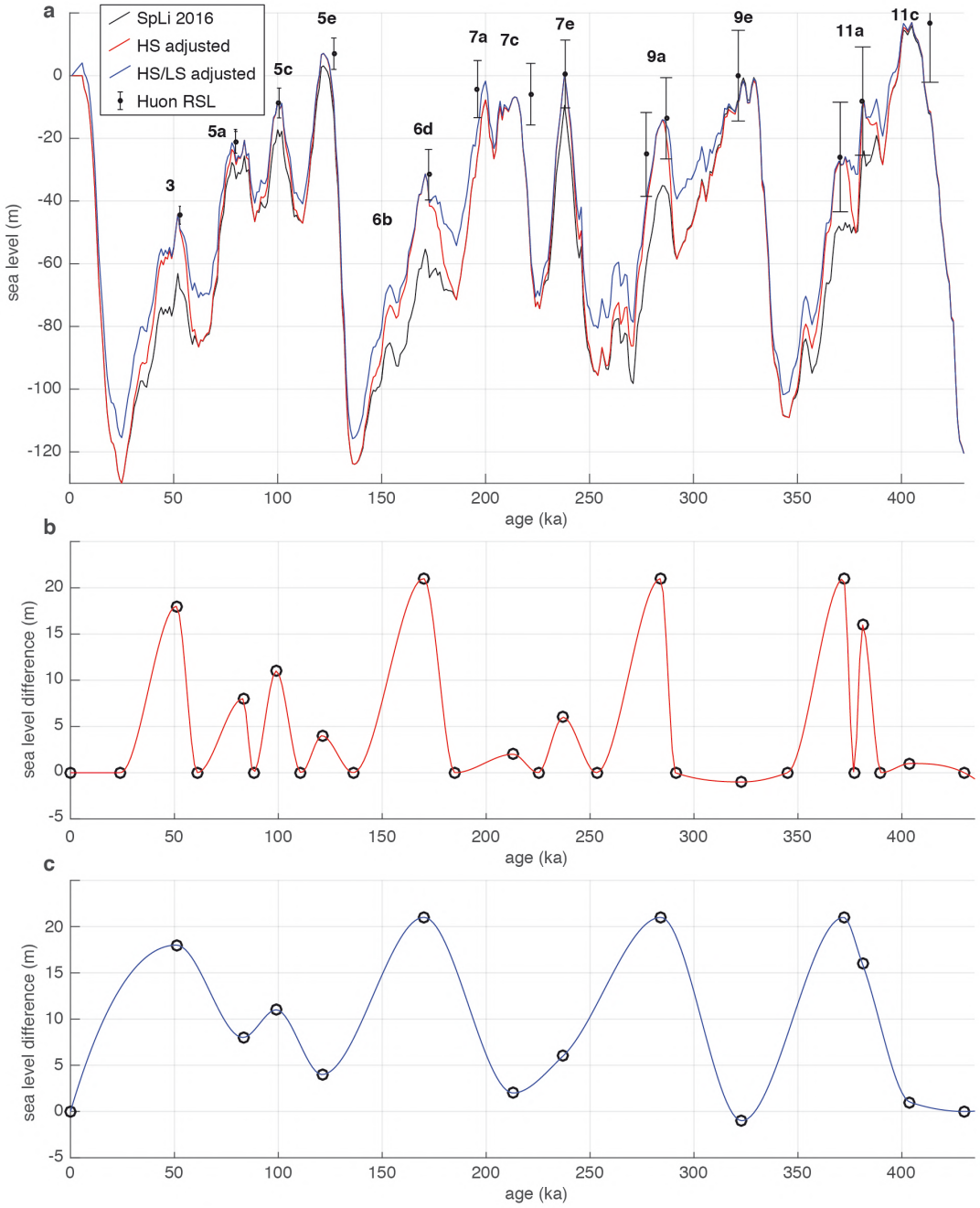

Supplementary Fig. 5: Modifying SL-curves. a) Sea-level curves used for terrace modelling, including the Spratt and Lisiecki (2016) GMSL curve (black), a modified version of that curve with only the highstands adjusted (red) and a modified version with both high- and lowstands adjusted (blue). Marine Isotope Stages are labeled in bold. **b)** Modifications applied to the highstand-adjusted curve in **a c)** Modifications applied to the high- and lowstand adjusted curve in **a**.

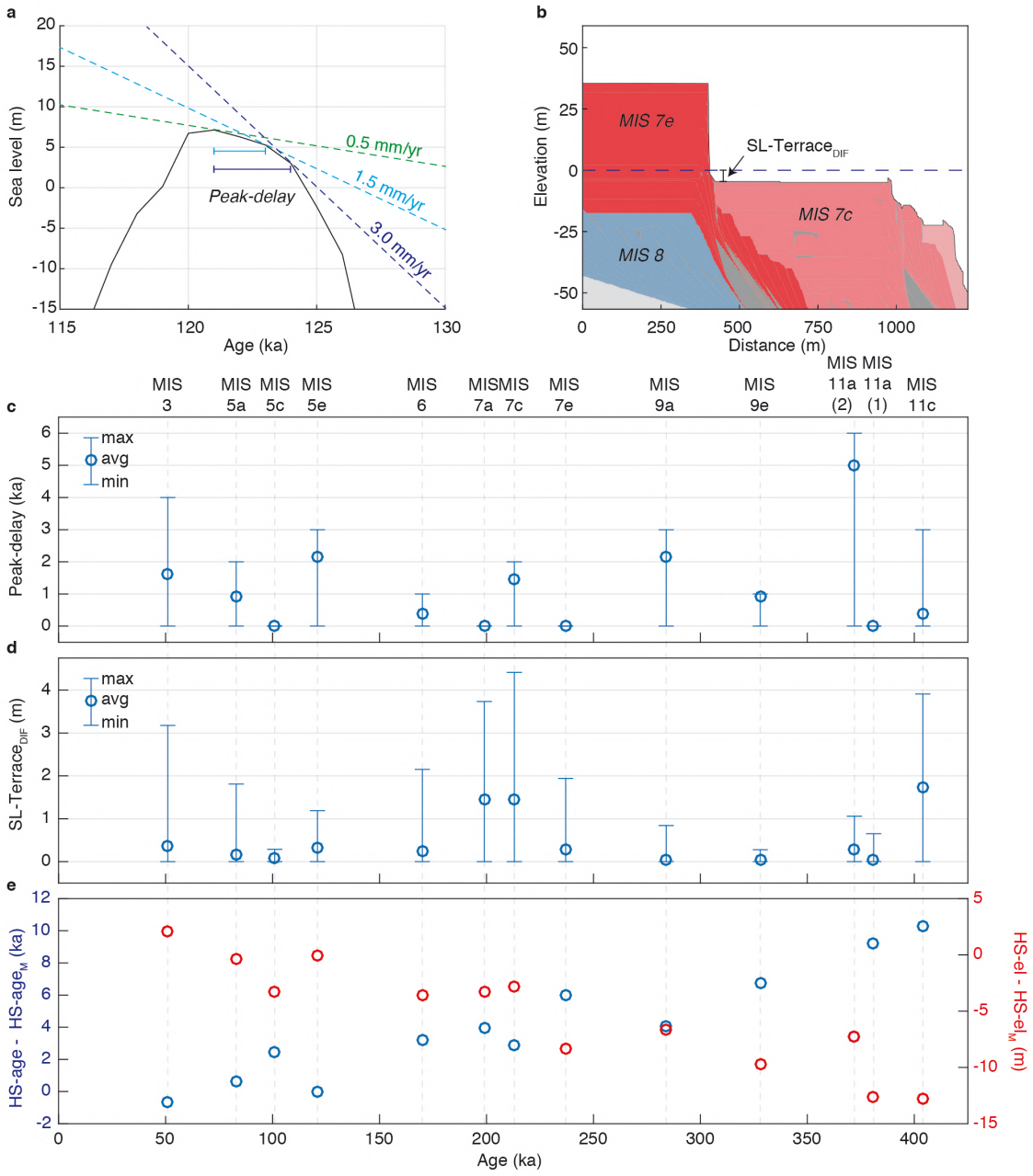

Supplementary Fig. 6: Model tests to quantify sea-level pitfalls. a) Example of MIS 5e sea-level highstand (highstand adjusted curve of Supplementary Fig. 5), showing how different uplift rates can result in different ages for maximum relative sea-level elevations (peak-delay) **b)** Example of MIS 7c reef forming ~4m meters below sea-level for an uplift rate of 1.5 mm/yr (SL-Terrace$_{DIF}$) **c)** Minimum, average and maximum peak-delay calculated for modelled SL-highstands for a range of 0.5-3.5 mm/yr, potential reef growth rate of 10 mm/yr and basal slopes similar to Huon stacked swath profiles (Supplementary Data 2) **d)** Minimum, average and maximum SL-TerraceDIF calculated with the same parameters as in **c e)** Effects of peak-delay and SL-Terrace$_{DIF}$ on highstand elevation and age estimates, using a forward modelling approach with the parameters in **c**, and inverting modelled shoreline angles following the same approach as in Fig. 2

Name	Age (ka)	Age Err (kyr)	RSL (m)	RSL Err (m)	MIS	Equiv. previous literature	Range dated samples (ka)
T2	32.12	5.87	-64.62	18.93	3 (7)	Reef IIb	33, 33
T3	37.35	2.38	-59.16	7.30	3 (6)	Reef IIa	35, 38, 42
T4	43.05	1.56	-56.21	4.54	3 (5)	Reef IIIc	
T5	44.13	1.03	-44.07	2.92	3 (4)	Reef IIIb	44, 45
T6	48.98	1.09	-45.88	3.15	3 (3)	Reef IIIal	55
T7	52.96	1.04	-44.52	2.86	3 (2)	Reef IIIam	51, 52
T8	59.68	1.17	-45.34	3.16	3 (1)	Reef IIIau	61
T9	69.96	1.19	-43.85	3.32	4	Reef IVb	65*, 68*, 70*, 72*
T10	74.70	1.29	-39.78	3.61	5a (3)	Reef IVa	65*, 68*, 70*, 72*
T11	79.71	1.38	-20.93	3.78	5a (2)	Reef Vb	93**, 93**
T12	86.32	2.26	-24.32	6.77	5a (1)	Reef Va	93**, 93**
T13	95.45	1.76	-28.91	4.91	5c (2)	Reef VIb	92, 99, 107, 113, 114, 118, 120***, 120***, 130, 138, 143
T14	100.69	1.77	-8.73	4.76	5c (1)	Reef VIa	90, 108, 113, 115, 120***, 120***, 126, 128, 129, 130, 130, 130, 131, 132, 133, 134,
T15	119.77	1.99	2.49	5.57	5e (2)	Reef VIIc	
T16	127	2	7	5	5e (1)	Reefs VIIa/VIIb	117, 118, 119, 137, 137
T17	157.30	3.42	-43.14	10.71	6b (2)	Reef VIII	
T18	165.15	3.03	-41.44	8.54	6b (1)	Reef VIII	
T19	172.58	2.90	-31.60	8.07	6d (2)	Reef VIII	
T20	186.52	3.17	-27.32	8.80	6d (1)	Reef IX	
T21	196.14	3.31	-4.29	9.10	7a	Reef IX	
T22	212.96	3.54	-7.16	9.70	7c (2)	Reef IX	
T23	221.74	3.63	-5.91	9.84	7c (1)	Reef IX	
T24	234.40	6.28	-11.97	16.14	7e (2)	Reef X	
T25	238.31	3.99	0.54	10.80	7e (1)	Reef X	
T26	277.24	5.19	-25.13	13.37	9a (2)		
T27	286.86	4.93	-13.59	12.97	9a (1)		
T28	321.53	5.48	0.01	14.48	9e		
T29	370.59	6.93	-25.94	17.48	11a (2)		
T30	381.42	6.78	-8.10	17.27	11a (1)		
T31	413.74	6.86	16.51	18.60	11c		

* Not specified if IVa or IVb
** Not specified if Va or Vb
*** Not specified if VIa or VIb

Supplementary Table 1: RSL Highstands Huon. MIS = Marine Isotope Stage, with substages as defined by Railsback et al. (2015). RSL = Relative Sea-Level elevations. Dated samples for Reefs II and III are taken from Chappell (2002), dated samples for the other Reefs from the compilation in Hibbert et al. (2016). VIIa and

VIIb are taken as one reef here, as VIIb appears to be the paleobarrier associated with VIIa (Esat et al., 1999). Bracketed numbers for MIS refer to the different RSL estimates within one MIS (1 for the oldest, etc.).

Location		Coral Reef Terrace			
Longitude (dec. deg.)	Latitude (dec. deg.)	UL [m]	LL [m]	IR [m]	RWL [m]
147.50	-6.00	-0.33	-0.97	0.64	-0.65
147.59	-6.07	-0.33	-0.97	0.64	-0.65
147.62	-6.10	-0.33	-0.98	0.66	-0.65
147.66	-6.15	-0.33	-0.99	0.66	-0.66
147.68	-6.18	-0.33	-0.99	0.66	-0.66
147.68	-6.21	-0.33	-0.99	0.67	-0.66
147.71	-6.25	-0.32	-0.99	0.67	-0.66
147.80	-6.31	-0.32	-1.00	0.68	-0.66
		Average			
		-0.33	-0.99	0.66	-0.66

Supplementary Table 2: Indicative range for coral reef terraces at Huon for present-day hydrodynamic conditions. Calculated for different locations along the coastal section using the indicative meaning calculator of Lorscheid and Rovere (2019). UL = Upper Limit, LL = Lower Limit, IR = Indicative Range, RWL = Reference Water Level

Previous work (Chappell, 1983; Chappell and Shackleton 1986; Lambeck and Chappell, 2001)

Name	Age (ka)	Age Err (ky)	Deposit Elev. (m)	Uplift Rate (mm/yr)	LS Elev. (m)	LS Err (m)
IIIa-base	47.5	2	91	3.3-3.5	-65	6
IVa-base	76	2	161	3.3-3.5	-65	10
Va-base	94	2	242	3.3-3.5	-56	8
VIa-base	103	3	277	3.3-3.5	-54	12
VIb-base	112.5	3	304	3.3-3.5	-61	9

Using uplift rates from this study

Name	Age (ka)	Age Err (ky)	Deposit Elev. (m)	Uplift Rate (mm/yr)	LS Elev. (m)	LS Err (m)
T5-base	46.6	2	91	3.075	-52.3	6
T9-base	72.3	2	161	3.115	-64.2	10
T12-base	90.9	2	242	3.145	-43.9	8
T13-base	98.1	3	277	3.156	-32.6	12
T14-base	110.2	3	304	3.175	-45.9	9

Supplementary Table 3: Tewai section lowstand calculation. LS = lowstand